Na-Dependent Ultrafast Carrier Dynamics of CdS/Cu(In,Ga)Se2 Measured by Optical Pump-Terahertz Probe Spectroscopy

ARTICLE *in* THE JOURNAL OF PHYSICAL CHEMISTRY C · JULY 2015

Impact Factor: 4.77 · DOI: 10.1021/acs.jpcc.5b02282

8 AUTHORS, INCLUDING:

Woo-Jung Lee

Electronics and Telecommunications Researc…

31 PUBLICATIONS **67** CITATIONS

SEE PROFILE

Dae-Hyung Cho

Electronics and Telecommunications Researc…

31 PUBLICATIONS **158** CITATIONS

SEE PROFILE

Yong-Duck Chung

Electronics and Telecommunications Researc…

103 PUBLICATIONS **636** CITATIONS

SEE PROFILE

THE JOURNAL OF PHYSICAL CHEMISTRY C

Article

pubs.acs.org/JPCC

Na-Dependent Ultrafast Carrier Dynamics of CdS/Cu(In,Ga)Se_2 Measured by Optical Pump-Terahertz Probe Spectroscopy

Woo-Jung Lee,[†] Dae-Hyung Cho,[†] Jae-Hyung Wi,[†] Won Seok Han,[†] Yong-Duck Chung,*[,†,‡] Jaehun Park,[§] Jung Min Bae,[∥] and Mann-Ho Cho[∥]

[†]Components & Materials Research Laboratory, Electronics and Telecommunications Research Institute, Daejeon 305-700, Korea

[‡]Department of Advanced Device Engineering, Korea University of Science and Technology, Daejeon 305-350, Korea

[§]fs-THz Laboratory, Pohang Accelerator Laboratory, POSTECH, Pohang 790-784, Korea

[∥]Insitute of Physics and applied physics, Yonsei University, Seoul120-749, Korea

Supporting Information

ABSTRACT: To investigate the origin of the Na effect on photovoltaic (PV) devices, Cu(In,Ga)Se_2 (CIGS) and CdS/CIGS layers were grown on borosilicate (BS) and soda-lime glass (SLG), respectively. The defect states and nonequilibrium carrier dynamics of the samples were measured using photoluminescence (PL) and optical pump-THz probe (OPTP) spectroscopy. From the PL results, we discovered that different shallow donor−acceptor levels were formed in the CIGS layer grown on BS and SLG, respectively. In the OPTP results, relaxation times of photocarriers excited from the CdS/CIGS layer were clearly distinguishable, and are explained by the formation of different defect states depending on substrates. In BS, deep defect level '*DX* states' were formed in the E_g near the p−n junction, which induce trapping photocarriers, resulting in shortening relaxation time. In SLG, there was no "*DX* state", which clearly demonstrates the positive effect of Na atoms at the p−n junction on performance of PV devices.

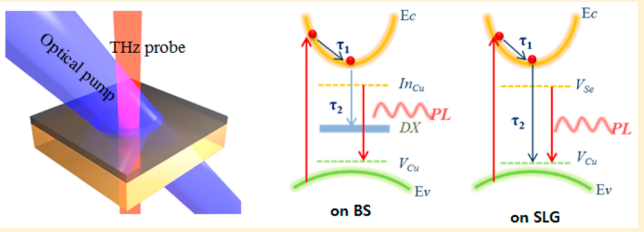

INTRODUCTION

I−III−VI_2 chalcopyrite semiconductors such as $CuInSe_2$, $CuGaSe_2$, and Cu(In,Ga)Se_2 (CIGS) are attractive materials for photovoltaic (PV) devices because of their beneficial qualities, including, for example, a high absorption coefficient for visible light, favorable direct bandgap (E_g), and great power conversion efficiency.[1−5] The CIGS comprised of $CuInSe_2$−$CuGaSe_2$ alloys in particular is considered to be the most efficient absorber material in a thin film PV device. The CIGS layer is generally deposited as a polycrystalline structure with an amount of native defect states and grain boundaries, which serve as carrier traps and recombination centers. These defect states have a decisive effect on the carrier relaxation dynamics in the CIGS layer, dominating the device performance.[6−8] Thus, to improve the CIGS efficiency in a PV device, it is essentially necessary to understand the intrinsic characteristics of the native defects in CIGS.

Na content is known to be one of the methods for enhancing the efficiency of a PV device.[9−12] Na atoms are typically supplied by utilizing soda-lime glass (SLG), which is a preferred substrate material for the industrial manufacturing of rigid CIGS-based modules.[13] During fabrication of the device, Na atoms diffuse from the SLG into the CIGS layer through a Mo layer, and this can beneficially affect the conversion efficiency of the PV device.[11] Although Na diffusion into the CIGS layer may alter the electronic structure and defect states, direct evidence of how Na influences the performance of PV devices has not yet been obtained experimentally. Considering that the CIGS layer has abundant intrinsic point defects, it is assumed that the electronic structure of defect states can be changed by Na content, which is a crucial issue in efforts to optimize PV device design.

In this paper, to investigate the formation of defect states in the CIGS layer depending on the Na content, a study of ultrafast carrier dynamics was conducted on the CIGS layers grown on two different substrates, borosilicate (BS) and SLG. Carrier dynamics related to defects can be determined by the relaxation times of the scattering rate or carrier-trapping at defect states, ranging from hundreds of femtoseconds to several picoseconds.[14,15] Among various measurement tools, optical pump-THz probe (OPTP) spectroscopy was utilized in this experiment because it is an extremely sensitive tool for investigating scattering mechanisms and dynamic energy transitions in the region of shorter time scales on the order of ∼femtoseconds and picoseconds.[15−20] A p−n junction was formed by depositing a CdS layer as a buffer layer, after which carrier dynamics were also subsequently analyzed. The measurement results revealed different relaxation mechanisms in the CIGS layers and CdS/CIGS layers depending on the substrate type, BS or SLG. The mechanisms were found to

Received: March 9, 2015
Revised: July 2, 2015

DOI: 10.1021/acs.jpcc.5b02282
J. Phys. Chem. C XXXX, XXX, XXX−XXX

result from the existence of deep defect levels, designated '*DX* states', in the case of BS, due to Na-deficiency, as compared to the SLG.

EXPERIMENTAL SECTION

p-type CIGS layers approximately 2.5 μm-thick were deposited with polycrystalline structure by a conventional coevaporation method using a three-stage process on Mo-coated BS (Na_2O: 4 atom %) and SLG (Na_2O: 14 atom %), respectively.[21] The [Ga]/([In]+[Ga]) and [Cu]/([In]+[Ga]) composition ratios of the CIGS layer were about 0.14 and 0.87 in both cases. As a buffer layer, an *n*-type CdS layer with a thickness of ~70 nm was grown on the CIGS via the chemical bath deposition method. Typical PV devices (ITO/i-ZnO/CdS/CIGS/Mo) were then fabricated on BS and SLG under identical conditions, and their efficiencies were determined to be 8.5% and 10.9%, respectively.[22] The device performance on SLG was superior to that on BS by ~2.4%, which is ascribed to the diffusion of Na atoms from the SLG.

To investigate how the substrates affected defect states, PL and OPTP measurements were conducted on CIGS and CdS/CIGS layers grown on BS and SLG without a Mo layer. For OPTP measurement, the terahertz (THz) signal should be transmitted through the material, and then detect absorbed signal. In the case of metal film, the THz signal is completely absorbed by free carriers of the metal, and therefore the samples are directly prepared on the substrate. Moreover, the Mo layer does not influence the Na-diffusion forward CIGS layer.[9,23]

The excitation laser source and power for the PL measurement were tuned to 400 nm and 2.5 mW, and the experiment was performed at a temperature below 15 K. A Ti:sapphire femtosecond regenerative amplifier system (Micra-Legend Elite, Coherent Inc.) was used for the time domain spectroscopy and the time-resolved THz spectroscopy in the OPTP measurement.[24] In this technique, after an ultrafast optical pulse of 400 nm excites the sample, the transient change of the sample in the 0.2−2.6 THz frequency range is probed by transferred THz pulses via electro-optic sampling. The time evolution of the OPTP signal is collected by scanning the time delay of the pump pulses with respect to the transferred THz pulse. All OPTP experiments were performed at room temperature in ambient dry air. More detailed information is described in Supporting Figure 1.

RESULTS AND DISCUSSION

Morphology and Atomic Concentration Measurement. Scanning electron microscope (SEM) measurement was performed on each CdS/CIGS samples grown on BS and SLG as shown in Figure 1a,b and Figure 1c,d, respectively. Approximately 2.5 μm-thick CIGS absorber and 70 nm-thick CdS buffer layer were similarly deposited on both substrates. We found out that grain size of CIGS grown on SLG is larger than that on BS. To verify the existence of the Na content, depth profiles of the elemental constituents in the CIGS layer and CdS/CIGS layer grown on BS and SLG were examined by using secondary ion mass spectroscopy (SIMS), respectively, as shown in Supporting Figure 2. The atomic distributions of elements into the CIGS layer are almost similar to each other, regardless of the substrates. A substantial Na content diffused up to the CdS layer in the SLG case, but not the BS, as indicated in Figure 2. SIMS results demonstrate that the SLG

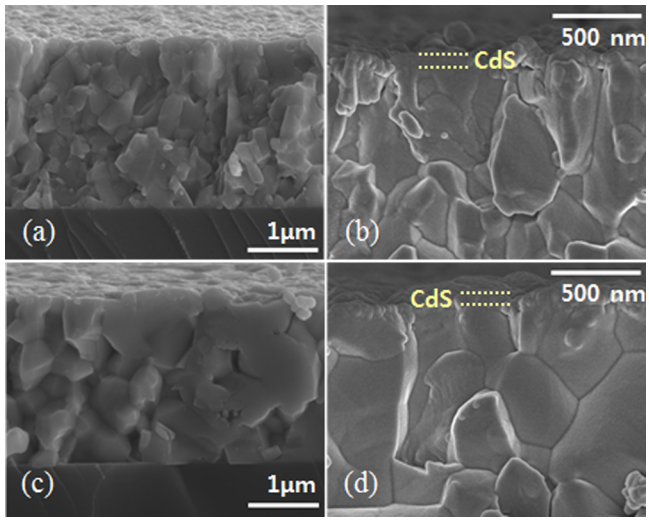

Figure 1. SEM images of CdS/CIGS film grown on BS (a,b) and SLG (c,d).

can effectively supply Na atoms into the CIGS and the CdS layer as compared to BS.

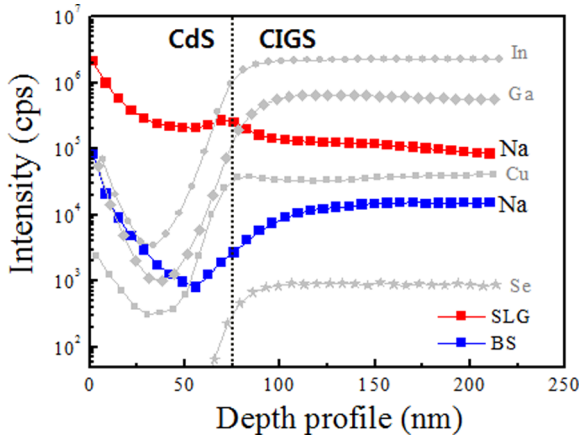

Figure 2. SIMS depth profiles of Na atoms in the CdS/CIGS layers grown on BS and SLG.

OPTP Spectroscopy Measurement. In our system as simply illustrated in Figure 3a, a Ti:sapphire regenerative amplifier is used to produce 1 kHz pulse train of 2.5 mJ and 800 nm pulses with a pulse duration of 120 fs (fwhm). The second harmonic (400 nm) of an amplified laser through a type-II β-Barium Borate (BBO) crystal is used as the pump beam. The pump beam fluence is approximately 560 $\mu J/cm^2$. THz probe pulse generation occurs via optical rectification of the fundamental pulse in a 10 × 10 mm ⟨110⟩ ZnTe crystal with a thickness of 1 mm.[25] The transmitted THz radiation is detected by means of an electro-optic (EO) sampling method in another 3 mm thick ⟨110⟩ ZnTe nonlinear crystal. Figure 3b shows the THz pulse spectra transmitted through the BS and SLG. After penetration of THz pulse through the substrate, the intensity of the THz pulse was drastically decreased as compared with the reference THz pulse (noted as "air"). Based on the results of the THz−TDs spectrum (refer to Supporting Figure 3), we measured the nonequilibrium carrier dynamics of the CIGS and CdS/CIGS layer using the OPTP spectroscopy. When an intense femtosecond laser pump pulse

DOI: 10.1021/acs.jpcc.5b02282
J. Phys. Chem. C XXXX, XXX, XXX−XXX

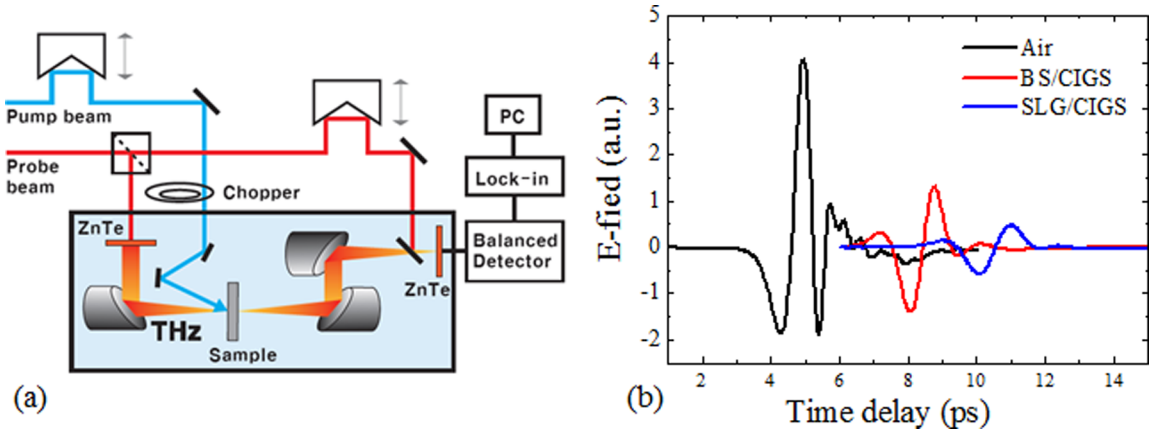

Figure 3. (a) A schematic diagram of the time-resolved THz spectrometer for the measurement of OPTP experiments. (b) THz pulse spectra transmitted through the BS and SLG with a reference THz pulse measured by THz−TDs spectroscopy.

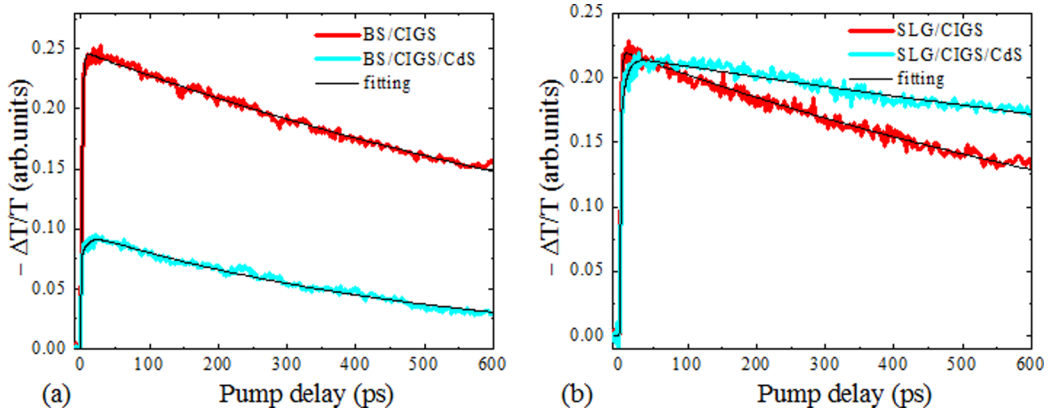

Figure 4. Measured (circles) and fitted (line) $-\Delta T/T$ spectra of the CIGS and CdS/CIGS layers grown on BS (a) and SLG (b) produced by the photoinduced change in the THz probe pulse (a 400 nm-pump beam was used).

of 400 nm is injected, charge carriers excite, and the THz probe pulse is transmitted with pump-induced change; i.e., the THz probe pulse transmitted through the samples reflects the absorption change induced by the femtosecond laser pump pulse of 400 nm, which is expressed as $-\Delta T/T$. The time evolution of the OPTP signal is collected by scanning the time delay of pump pulses with respect to the transferred THz pulse. Thus, the near-edge $-\Delta T/T$ spectra intensity implies the photoexcited carrier density, and the decay curve corresponds to the carrier lifetime. The $-\Delta T/T$ signal is mainly attributed to the carrier relaxation of photoexcited electrons ("photo-carrier") since the effective mass of the electron is smaller than that of a hole in $CuInSe_2$ and $CuGaSe_2$.[26] The typical $-\Delta T/T$ curve, at first, abruptly increases due to the absorption of photoexcited carriers by photon energy above the E_g, and then sequentially decays owing to the intraband relaxation (τ_1) and the recombination process/trapping at defect states (τ_2) (Figure 4).[14,15] The more detailed relaxation mechanism is explained in Supporting Figure 4. Notably, we found that the photocarrier density is drastically decreased after the deposition of CdS layer in the case of BS and is almost identical to both CIGS and CdS/CIGS layers in the case of SLG, which means that the characteristics of the CIGS layer are significantly changed in contact with the CdS layer. The time evolution of $-\Delta T/T$ can be well fitted with a biexponential function (the equation is shown in Supporting Figure 1). The lifetimes of τ_1 and τ_2 obtained from the CIGS layer were approximately 1.7 and 1150 ps in BS, and 1.3 and 1110 ps in SLG; this means that a similar relaxation mechanism exists in the two CIGS layers. After deposition of the CdS layer, the lifetimes of τ_1 and τ_2 were noticeably changed into 9.3 and 520 ps in BS, and 7.6 and 2580 ps in SLG. Interestingly, τ_2 dropped by half in BS, whereas it rose 2-fold in SLG. These lifetimes are summarized in Table 1.

Table 1. Carrier Lifetimes Obtained from the CdS/CIGS and CIGS Layer Are Summarized as a Function of Substrate

				(±0.1 ps)
	BS/CIGS	BS/CIGS/CdS	SLG/CIGS	SLG/CIGS/CdS
τ_1	1.7 ps	9.3 ps	1.3 ps	7.6 ps
τ_2	1150 ps	520 ps	1110 ps	2580 ps

PL Measurement. To identify the defect states determining the lifetime of the relaxed carriers, PL measurement was performed with an excitation light of 400 nm, an identical value to the pump beam energy of OPTP. Figure 5 indicates the PL spectra obtained from the CIGS and CdS/CIGS layer on BS and SLG. The results clearly demonstrate that a different optical transition occurs for the two substrates. Moreover, based on PL intensity, we assumed that the performance of PV devices on SLG would be superior to those on BS because the radiative recombination rate was much higher in the case of SLG. After deposition of the CdS layer, radiative recombination is decreased in BS, whereas it is increased in SLG, which is

DOI: 10.1021/acs.jpcc.5b02282
J. Phys. Chem. C XXXX, XXX, XXX−XXX

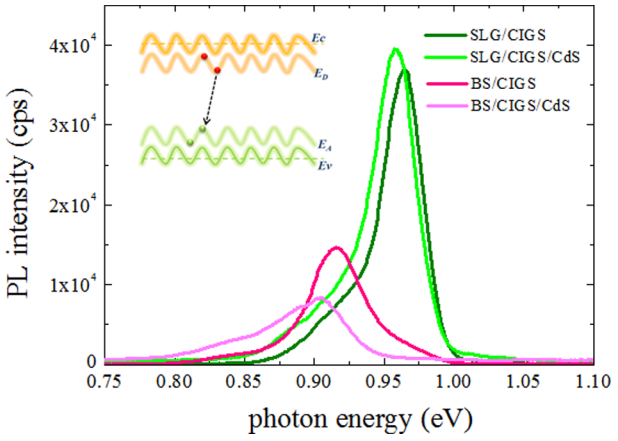

Figure 5. PL spectra obtained from the CIGS and CdS/CIGS layer grown on BS and SLG with excitation energy of 400 nm. Inset shows the potential fluctuation of band diagram due to the numerous point and ordered defects.

evidence for higher efficiency of the PV device on SLG. In the Cu-poor CIGS layer, PL emission was governed by localized carriers in donor and acceptor states below the band edge due to abundant native point defects; i.e., the PL peak assigned to the donor–acceptor pair (DAP) transition.[27−30] The DAP transition energy is measured of approximately 0.97 and 0.92 eV in CIGS on SLG and BS, respectively. Using the estimated E_g of 1.1 eV (refer to Supporting Figure 5), the sum of each donor and acceptor ionization energy ($\Delta E_D + \Delta E_A$) becomes 130 meV in SLG and 180 meV in BS. According to several reports, the enthalpy of the formation energy of defects such as V_{Cu}^-, V_{Se}^+, and In_{Cu}^- is very small and even negative.[26,31] In the CIGS layer on SLG, the PL peak of 0.97 eV stems from the optical transition between the shallow acceptor level of 50 meV formed by Cu vacancies (V_{Cu}) and the donor level of 80 meV created by the Se vacancy (V_{Se}).[29] In CIGS on BS, a new defect level emerges. It is plausible to assign this as an optical transition from antisite In_{Cu} as a donor level of descending order to V_{Cu}.[29,32] After deposition of the CdS layer, redshift of the PL peaks was observed in both cases. This could be explained by the potential fluctuation that occurs in compensated semiconductors, such as the Cu-poor CIGS compound with ordered defect arrays, which has neutral defect ($In_{Cu} - 2V_{Cu}$) pairs compensating for opposite sites.[33,34] In the CIGS layer, charged acceptors and donors are randomly distributed into spatially separated potential wells, leading to potential fluctuation, which in turn brings about band bending as shown in the inset of Figure 5. This phenomenon is intensified at a p–n junction. Thus, a captured carrier at an impurity site can have not only direct recombination, but prior to recombination, transfer to a state lower in energy, resulting in redshift with peak broadening.

Carrier Decay Kinetics in CIGS. Generally, photocarriers excited by high photon energy comply with Fermi–Dirac distributions through carrier–carrier scattering within a few hundred femtoseconds, and then lose their excess energy to the lattice, and relax to the bottom of the band by carrier-phonon scattering within several picoseconds.[14,15] In both cases of CIGS on BS and SLG, τ_1 shows a similar trend regardless of substrate types because τ_1 is determined by the intraband relaxation time to reach at bottom of the conduction band; i.e., it means that CIGS layers grown on BS and SLG are almost identical. Moreover, measured lifetimes of τ_1 in our system are similar to other results reported for CIGS thin film.[23,35] On the other hand, τ_2 corresponds to an interband relaxation time either by the recombination of the electron–hole pair to restore initial states or by the electron trapping at defect states energetically located within the E_g.[14,15] The both τ_2 obtained from the CIGS on BS and SLG also indicate similar values. Considering reported lifetimes, τ_2 is ascribed to the relaxation time from conduction band edge to the shallow acceptor energy level localized above the valence band edge within several nanoseconds.[23]

Carrier Relaxation Mechanism at p–n Junction of CdS/CIGS. After the p–n junction is formed, τ_1 becomes longer within several picoseconds in both cases of CdS/CIGS on BS and SLG. This is due to the CdS band structure with larger E_g of 2.4 eV, bringing about rise of the time for photocarriers to reach at conduction band edge. On the other hand, τ_2 exhibited the opposite trend after the deposition of the CdS layer on CIGS, which implies that different defect states are formed near the p–n junction as a function of substrate type. In BS, τ_2 is about 520 ps, whereas in SLG, it is approximately 2580 ps; i.e., in the case of BS, a deeper defect level to trap photocarriers could be formed at the p–n junction, shortening the τ_2 value. Considering PL results of Figure 5, the formation of deeper defect states into the E_g is plausible in CIGS on BS because decreased PL intensity is caused by electron trapping at defect states instead of the radiative recombination. We suggest that the Na atoms can affect the quality of p–n junctions and defect states located in E_g. According to calculation results, ionized intrinsic In_{Cu}^{2+} can transform into lattice-relaxed, deep defect level '*DX* states' formed as a Frenkel-pair consisting of an In interstitial and a Cu vacancy; i.e., $In_{Cu}^{2+} + 2e \rightarrow In_{DX}^{0} = (In_i^+ - V_{Cu}^-)$.[36] Since large quantities of isolated In_{Cu} and isolated V_{Cu} are formed very close to a 1:2 ratio during CIGS growth, most In_{Cu} eventually exists as a neutral defect ($In_{Cu} - 2V_{Cu}$), whereas the amount of uncompensated isolated In_{Cu} becomes a donor.[37,38] The above intrinsic defect complexes can create the defect-localized states in the E_g, namely '*DX* states', in the case of $Cu(In_{1-x}Ga_x)Se_2$ with an $E_g \leq 1.2$ eV and $x < 0.3$.[36] This has a harmful influence on PV device performance by trapping photocarriers produced by photoexcitation under illumination. These '*DX* states' even cause Fermi level pinning and trapping of photocarriers near the p–n junction, resulting in a decrease of τ_2 in BS. In the case of SLG, the increase of τ_2 is thought to result because the added Na automatically diffuses into the CIGS and CdS layer from the SLG, as demonstrated in Figure 2. The incorporation of less than 1% Na is considered enough to significantly change their electronic properties. Na is known to reduce the defect density in CIGS film by passivation of the Se vacancy or annihilation of the compensating antisite donor defect In_{Cu} by Na.[10,30] We suggest a possible scenario for the cause of the longer lifetime, τ_2 in SLG: (i) Na eliminates In_{Cu} by substituting for In on Cu sites; i.e., forming Na_{Cu} and (ii) Na easily forms Na_{In} antisite defects, resulting in an increase in acceptor density.[30,39] Thus, there is no '*DX* state' in SLG, which is due to the deficient In_{Cu} being replaced by Na_{Cu}, which prevents the creation of defect complexes ($In_{Cu} - 2V_{Cu}$) near the p–n junction. In other words, the introduction of Na into the CIGS and CdS layers plays an important role in the PV device; this is because of the removal of '*DX* states' and an increase in acceptors, thereby promoting τ_2 in SLG. The relaxation mechanism of photocarriers at the p–n junction of CdS/CIGS depending on the two substrates of BS and SLG is displayed in a simplified band

DOI: 10.1021/acs.jpcc.5b02282
J. Phys. Chem. C XXXX, XXX, XXX–XXX

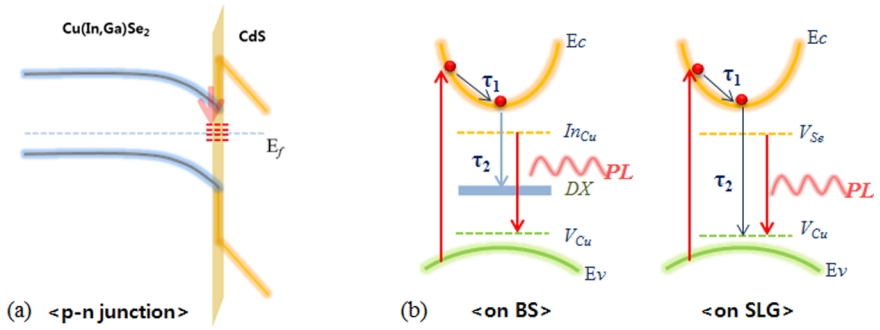

Figure 6. (a) A schematic defect level diagram at the p−n junction of CdS/CIGS. (b) Illustration of the carrier relaxation mechanism of CIGS thin films after deposition of CdS layer depending on substrate type of BS and SLG.

structure in Figure 6. This result clearly indicates that Na atoms exert a positive effect at the p−n junction of PV devices by producing increased photocarrier lifetimes in the case of SLG.

CONCLUSIONS

In summary, we have briefly demonstrated the effectiveness of OPTP measurement for determining the ultrafast carrier dynamics of photocarriers excited from CIGS and CdS/CIGS layers depending on substrates types. Through optical transition of the PL spectra, we discovered that distinguishable defect states were formed as the donor levels of In_{Cu} in BS and V_{Se} in SLG. From the extracted carrier lifetimes, we found that the defect states were significantly changed after the formation of the p−n junction. Considering the enthalpy of formation energy, a deep complex defect level of $(In_{Cu} - 2V_{Cu})$ designated '*DX* states' could be natively formed in the E_g near the p−n junction in the case of BS, resulting in a decrease of τ_2 by trapping photocarriers. By contrast, τ_2 was increased in SLG with the addition of a Na supply, which is considered to relieve the defect level located in the E_g, forming the Na_{Cu} antisite.

ASSOCIATED CONTENT

Supporting Information

Measurement of optical pump-THz probe spectroscopy; SIMS depth profiles of elemental constituents in the CIGS and CdS/CIGS layers grown on BS and SLG; THz pulse spectra transmitted through the BS and SLG; relaxation mechanism of the photoexcited carrier in the semiconductor after injection of an optical pump beam above band gap; and bandgap energy of 1.1 eV obtained from the transmission spectrum. The Supporting Information is available free of charge on the ACS Publications website at DOI: 10.1021/acs.jpcc.5b02282.

AUTHOR INFORMATION

Corresponding Author

*E-mail: ydchung@etri.re.kr.

Notes

The authors declare no competing financial interest.

ACKNOWLEDGMENTS

Terahertz spectroscopy was performed using the fs-THz beamline at the Pohang Light Source (PLS). This work was supported by the R&D pioneer program of ETRI and 'New & Renewable Energy' Korea Institute of Energy Technology Evaluation and Planning (KETEP) grants funded by the Korean government Ministry of Trade, Industry & Energy (Nos. 20123030010030, 20153010011990). The authors also would like to acknowledge the financial support from the R&D Convergence Program of MSIP (Ministry of Science, ICT and Future Planning) and ISTK (Korea Research Council for Industrial Science and Technology) of the Republic of Korea (Grant B551179-12-01-00).

REFERENCES

(1) Gabor, A. M.; Tuttle, J. R.; Albin, D. S.; Contreras, M. A.; Noufi, R.; Hermann, A. M. High-efficiency $CuInxGa_{1-x}Se_2$ solar cells made from $(In_xGa_{1-x})_2Se_3$ precursor films. *Appl. Phys. Lett.* **1994**, *65*, 198−200.

(2) Persson, C.; Zhao, Y.-J.; Lany, S.; Zunger, A. *n*-type doping of $CuInSe_2$ and $CuGaSe_2$. *Phys. Rev. B: Condens. Matter Mater. Phys.* **2005**, *72*, 035211.

(3) Repins, I.; Contreras, M. A.; Egaas, B.; DeHart, C.; Scharf, J.; Perkins, C. L.; To, B.; Noufi, R. 19·9%-efficient ZnO/CdS/$CuInGaSe_2$ solar cell with 81·2% fill factor. *Prog. Photovoltaics* **2008**, *16*, 235−239.

(4) Jackson, P.; Hariskos, D.; Lotter, E.; Paetel, S.; Wuerz, R.; Menner, R.; Wischmann, W.; Powalla, M. New world record efficiency for Cu(In,Ga)Se_2 thin-film solar cells beyond 20%. *Prog. Photovoltaics* **2011**, *19*, 894−897.

(5) Park, N.-M.; Lee, H. S.; Kim, J. Reactive sputtering process for $CuIn_{1-x}Ga_xSe_2$ thin film solar cells. *ETRI Journal* **2012**, *34*, 779−782.

(6) Mönig, H.; Smith, Y.; Caballero, R.; Kaufmann, C. A.; Lauermann, I.; Lux-Steiner, M. C.; Sadewasser, S. Direct evidence for a reduced density of deep level defects at grain boundaries of Cu(In,Ga)Se_2 thin films. *Phys. Rev. Lett.* **2010**, *105*, 116802.

(7) Ohnesorge, B.; Weigand, R.; Bacher, G.; Forchel, A.; Riedl, W.; Karg, F. H. Minority-carrier lifetime and efficiency of Cu(In,Ga)Se_2 solar cells. *Appl. Phys. Lett.* **1998**, *73*, 1224−1226.

(8) Hafemeister, M.; Siebentritt, S.; Albert, J.; Lux-Steiner, M. C.; Sadewasser, S. Large neutral barrier at grain boundaries in chalcopyrite thin films. *Phys. Rev. Lett.* **2010**, *104*, 196602.

(9) Ishizuka, S.; Yamada, A.; Islam, M. M.; Shibata, H.; Fons, P.; Sakurai, T.; Akimoto, K.; Niki, S. Na-induced variations in the structural, optical, and electrical properties of Cu(In,Ga)Se_2 thin films. *J. Appl. Phys.* **2009**, *106*, 034908.

(10) Kronik, L.; Cahen, D.; Schock, H. W. Effects of sodium on polycrystalline Cu(In,Ga)Se_2 and its solar cell performance. *Adv. Mater.* **1998**, *10*, 31−36.

(11) Rudmann, D.; da Cunha, A. F.; Kaelin, M.; Kurdesau, F.; Zogg, H.; Tiwari, A. N.; Bilger, G. Efficiency enhancement of Cu(In,Ga)Se2 solar cells due to post-deposition Na incorporation. *Appl. Phys. Lett.* **2004**, *84*, 1129−1131.

(12) Cho, D.-H.; Lee, K.-S.; Chung, Y.-D.; Kim, J.-H.; Park, S.-J.; Kim, J. Electronic effect of Na on Cu(In,Ga)Se_2 solar cells. *Appl. Phys. Lett.* **2012**, *101*, 023901.

(13) Nakada, T. Invited Paper: CIGS-based thin film solar cells and modules: Unique material properties. *Electron. Mater. Lett.* **2012**, *8*, 179−185.

DOI: 10.1021/acs.jpcc.5b02282
J. Phys. Chem. C XXXX, XXX, XXX−XXX

(14) Othonos, A. Probing ultrafast carrier and phonon dynamics in semiconductors. *J. Appl. Phys.* **1998**, *83*, 1789−1830.
(15) Ulbricht, R.; Hendry, E.; Shan, J.; Heinz, T. F.; Bonn, M. Carrier dynamics in semiconductors studied with time-resolved terahertz spectroscopy. *Rev. Mod. Phys.* **2011**, *83*, 543−586.
(16) Prasankumar, R. P.; Upadhya, P. C.; Taylor, A. J. Ultrafast carrier dynamics in semiconductor nanowires. *Phys. Status Solidi B* **2009**, *246*, 1973−1995.
(17) Grumstrup, E. M.; Cating, E. M.; Gabriel, M. M.; Pinion, C. W.; Christesen, J. D.; Kirschbrown, J. R.; Vallorz, E. L., III; Cahoon, J. F.; Papanikolas, J. M. Ultrafast carrier dynamics of silicon nanowire ensembles: the impact of geometrical heterogeneity on charge carrier lifetime. *J. Phys. Chem. C* **2014**, *118*, 8626−8633.
(18) Grumstrup, E. M.; Gabriel, M. M.; Cating, E. M.; Pinion, C. W.; Christesen, J. D.; Kirschbrown, J. R.; Vallorz, E. L., III; Cahoon, J. F.; Papanikolas, J. M. Ultrafast carrier dynamics in individual silicon nanowires: characterization of diameter-dependent carrier lifetime and surface recombination with pump−probe microscopy. *J. Phys. Chem. C* **2014**, *118*, 8634−8640.
(19) Tiwana, P.; Parkinson, P.; Johnston, M. B.; Snaith, H. J.; Herz, L. M. Ultrafast terahertz conductivity dynamics in nesoporous TiO_2: influence of dye sensitization and surface treatment in solid-state dye-sensitized solar cells. *J. Phys. Chem. C* **2010**, *114*, 1365−1371.
(20) Liu, H.; Lu, J.; Teoh, H. F.; Li, D.; Feng, Y. P.; Tang, S. H.; Sow, C. H.; Zhang, X. Defect engineering in CdS_xSe_{1-x} nanobelts: an insight into carrier relaxation dynamics via optical pump−terahertz probe spectroscopy. *J. Phys. Chem. C* **2012**, *116*, 26036−26042.
(21) Chung, Y.-D.; Cho, D.-H.; Han, W.-S.; Park, N.-M.; Lee, K.-S.; Kim, J.-H. Incorporation of Cu in $Cu(In,Ga)Se_2$-based thin-film solar cells. *J. Korean Phys. Soc.* **2010**, *57*, 1826−1830.
(22) Cho, D.-H.; Chung, Y.-D.; Lee, K.-S.; Park, N.-M.; Kim, K.-H.; Choi, H.-W.; Kim, J. Influence of growth temperature of transparent conducting oxide layer on $Cu(In,Ga)Se_2$ thin-film solar cells. *Thin Solid Films* **2012**, *520*, 2115−2118.
(23) Okano, M.; Takabayashi, Y.; Sakurai, T.; Akimoto, K.; Shibata, H.; Niki, S.; Kanemitsu, Y. Slow intraband relaxation and localization of photogenerated carriers in $CuIn_{1-x}Ga_xSe_2$ thin films: Evidence for the existence of long-lived high-energy carriers. *Phys. Rev. B: Condens. Matter Mater. Phys.* **2014**, *89*, 195203.
(24) Park, J.; Kim, C.; Lee, J.; Yim, C.; Kim, C. H.; Lee, J.; Jung, S.; Ryu, J.; Kang, H.-S.; Joo, T. Generation, transport, and detection of linear accelerator based femtosecond-terahertz pulses. *Rev. Sci. Instrum.* **2011**, *82*, 013305.
(25) Faure, J.; Van Tilborg, J.; Kaindl, R.; Leemans, W. Modelling laser-based table-top THz sources: optical rectification, propagation and electro-optic sampling. *Opt. Quantum Electron.* **2004**, *36*, 681−697.
(26) Zhang, S.; Wei, S.-H.; Zunger, A.; Katayama-Yoshida, H. Defect physics of the $CuInSe_2$ chalcopyrite semiconductor. *Phys. Rev. B: Condens. Matter Mater. Phys.* **1998**, *57*, 9642−9656.
(27) Dirnstorfer, I.; Wagner, M.; Hofmann, D.; Lampert, M.; Karg, F.; Meyer, B. Characterization of $CuIn(Ga)Se_2$ thin films. *Phys. Status Solidi A* **1998**, *168*, 163−175.
(28) Bacewicz, R.; Zuk, P.; Trykozko, R. Photoluminescence study of $ZnO/CdS/Cu(In,Ga)Se_2$ solar cells. *Opto-Electron. Rev.* **2003**, 277−280.
(29) Shirakata, S.; Ohkubo, K.; Ishii, Y.; Nakada, T. Effects of CdS buffer layers on photoluminescence properties of $Cu(In,Ga)Se_2$ solar cells. *Sol. Energy Mater. Sol. Cells* **2009**, *93*, 988−992.
(30) Shin, Y. M.; Lee, C. S.; Shin, D. H.; Ko, Y. M.; Al-Ammar, E. A.; Kwon, H. S.; Ahn, B. T. Characterization of $Cu(In,Ga)Se_2$ solar cells grown on Na-free glass with an NaF layer on a Mo film. *ECS J. Solid State Sci. Technol.* **2013**, *2*, P248−P252.
(31) Wei, S.-H.; Zhang, S. B.; Zunger, A. Effects of Ga addition to $CuInSe_2$ on its electronic, structural, and defect properties. *Appl. Phys. Lett.* **1998**, *72*, 3199−3201.
(32) Zott, S.; Leo, K.; Ruckh, M.; Schock, H. W. Photoluminescence of polycrystalline $CuInSe_2$ thin films. *Appl. Phys. Lett.* **1996**, *68*, 1144−1146.
(33) Levanyuk, A. P.; Osipov, V. V. Edge luminescence of direct-gap semiconductors. *Sov. Phys. Usp.* **1981**, *24*, 187.
(34) Liao, Y.-K.; Kuo, S.-Y.; Lin, W.-T.; Lai, F.-I.; Hsieh, D.-H.; Tsai, M.-A.; Chen, S.-C.; Chiou, D.-W.; Chang, J.-C.; Wu, K.-H.; et al. Observation of unusual optical transitions in thin-film $Cu(In,Ga)Se_2$ solar cells. *Opt. Express* **2012**, *20*, A836−A842.
(35) Chen, S.-C.; Liao, Y.-K.; Chen, H.-J.; Chen, C.-H.; Lai, C.-H.; Chueh, Y.-L.; Kuo, H.-C.; Wu, K.-H.; Juang, J.-Y.; Cheng, S.-J.; et al. Ultrafast carrier dynamics in $Cu(In,Ga)Se_2$ thin films probed by femtosecond pump-probe spectroscopy. *Opt. Express* **2012**, *20*, 12675−12681.
(36) Lany, S.; Zunger, A. Intrinsic DX centers in ternary chalcopyrite semiconductors. *Phys. Rev. Lett.* **2008**, *100*, 016401.
(37) Zhao, Y.-J.; Persson, C.; Lany, S.; Zunger, A. Why can $CuInSe_2$ be readily equilibrium-doped n-type but the wider-gap $CuGaSe_2$ cannot? *Appl. Phys. Lett.* **2004**, *85*, 5860−5862.
(38) Lany, S.; Zhao, Y.-J.; Persson, C.; Zunger, A. Halogen n-type doping of chalcopyrite semiconductors. *Appl. Phys. Lett.* **2005**, *86*, 042109.
(39) Niles, D. W.; Ramanathan, K.; Hasoon, F.; Noufi, R.; Tielsch, B. J.; Fulghum, J. E. Na impurity chemistry in photovoltaic CIGS thin films: Investigation with x-ray photoelectron spectroscopy. *J. Vac. Sci. Technol., A* **1997**, *15*, 3044−3049.

DOI: 10.1021/acs.jpcc.5b02282
J. Phys. Chem. C XXXX, XXX, XXX−XXX